

Timing of eclogite facies metamorphism in the southernmost Scandinavian Caledonides by Lu–Hf and Sm–Nd geochronology

Matthijs A. Smit · Erik E. Scherer ·
Michael Bröcker · Herman L. M. van Roermund

Received: 22 April 2009 / Accepted: 10 August 2009 / Published online: 28 August 2009
© Springer-Verlag 2009

Abstract The Scandinavian Caledonides contain several non-cogenetic eclogite-bearing terranes that were metamorphosed before the main orogenic stage in Scandian time (430–395 Ma). Although petrological and geochronological data from these terranes have provided essential information on the geodynamic history of the Caledonian orogenic cycle, the general picture is still patchy. To refine existing geodynamic models, we have dated the eclogite occurrence in the Jæren nappe, SW Norway, by Lu–Hf and Sm–Nd geochronology. Five out of the six studied samples provide a weighted mean Lu–Hf age of 469.9 ± 1.2 Ma ($\pm 2\sigma$). One sample provided a significantly younger age of 457.9 ± 2.4 Ma. Garnet from the younger sample grew exclusively at eclogite facies conditions. In contrast, garnet from the other samples comprises prograde cores and peak metamorphic rims. Age estimates that take Lu-contributions of each zone into account provide an age of 471.0 ± 0.9 Ma for the cores and suggest a ca. 455 Ma age for the rims, which is identical to the bulk-garnet age of the younger sample. The same pattern is indicated by Sm–Nd ages, although these are relatively imprecise and reflect isotopic disturbance during thermal overprinting upon

exhumation. The data define a new high-pressure age population for the Scandinavian Caledonides, which allows more detailed insight into the subduction history that affected the Baltoscandian margin before Scandian continental collision. Furthermore, this study highlights the potential complexities involved in garnet geochronology and shows the strength of Lu–Hf dating for unraveling the geochronological record of HP rocks.

Keywords Eclogite · Geochronology · Lu–Hf · Sm–Nd · Caledonides · Norway

Introduction

The Scandinavian Caledonides comprise several eclogite-bearing terranes, which occur along the >2,000 km long axis of the orogen (Griffin et al. 1985; Bryhni and Andréasson 1985; Brueckner and van Roermund 2004). Such terranes represent fossil subduction zones and are therefore key targets for studying the geodynamic history of orogenic belts. The best known of these is the archetypal high- and ultrahigh pressure (HP and UHP) terrane of the Western Gneiss Complex (WGC) in western Norway, which is a spectacular example of a Proterozoic crustal fragment that was reworked during the Caledonian cycle by subduction to depths up to 200 km (e.g., Scambelluri et al. 2009; van Roermund 2009). The WGC has provided detailed insight into the processes that occur during deep burial and exhumation of continental crust in collision zones (e.g., Terry and Robinson 2004; Brueckner and van Roermund 2004; Tucker et al. 2004; Root et al. 2005; Kylander-Clark et al. 2008, 2009; Spengler et al. 2009). As shown by numerous geochronological studies that used various isotope systems having different closure

Communicated by J. Hoefs.

Electronic supplementary material The online version of this article (doi:10.1007/s00410-009-0440-3) contains supplementary material, which is available to authorized users.

M. A. Smit (✉) · E. E. Scherer · M. Bröcker
Institut für Mineralogie, Westfälische Wilhelms-Universität,
Corrensstrasse 24, 48149 Münster, Germany
e-mail: m.a.smit@uni-muenster.de

H. L. M. van Roermund
Faculteit Geowetenschappen, Universiteit Utrecht, Budapestlaan
4, 3584 CD, Utrecht, The Netherlands

temperature, the HP and UHP metamorphism of the WGC is related to the Scandian orogeny (e.g., Griffin and Brueckner 1980; Tucker et al. 1990, 2004; Carswell et al. 2003; Root et al. 2004; Kylander-Clark et al. 2007, 2008, 2009; Glodny et al. 2008a; Spengler et al. 2009). Other eclogite occurrences are found in various tectonic units of the Caledonian thrust belt that separates the WGC from the Baltic Crystalline Shield (BCS, Fig. 1). Geochronological studies indicate that eclogitization in these units occurred during several (U)HP stages between 505 and 430 Ma (Mørk et al. 1988; Corfu et al. 2003; Brueckner and van Roermund 2007; Glodny et al. 2008b). These data suggest that the Scandinavian Caledonides are an amalgamation of different HP and UHP terranes that record several possibly independent subduction–eduction cycles (Brueckner and van Roermund 2004).

In contrast to many other (U)HP occurrences in this orogen, the eclogites of the Jæren nappe, SW Norway (Fig. 1) have not been previously dated. The regional correlation of this occurrence to eclogite-bearing terranes to the north (Bergen Arcs, WGC) is unknown, i.e., it is unclear whether this tectonic subunit is a lateral continuation of other (U)HP terranes or if it is a distinct sub-unit with its own unique tectono-metamorphic history. To constrain the HP age of the Jæren eclogites, we subjected these rocks to a detailed Lu–Hf and Sm–Nd geochronological study. Interpretation of the resulting age data takes into account contributions of different garnet growth zones that were identified by major- and trace element analysis.

This approach provides valuable insight into the tectono-metamorphic evolution of the south Scandinavian Caledonides and deepens the understanding of the (U)HP history of the Caledonian orogenic belt.

Geological setting and geochronological background

The Scandinavian Caledonides comprise a large NNE- to SSW-trending allochthonous thrust belt that was transported from west to east onto the western margin of the Baltic Crystalline Shield (Fig. 1). The orogen formed as a result of early- to mid-Palaeozoic convergence between the protocontinents Laurentia and Baltica and concomitant destruction of the intervening Iapetus Ocean. Final continental collision occurred during the Scandian orogeny (Roberts and Gee 1985), resulting in the westward continental subduction of Baltica underneath Laurentia. These final stages of the Caledonian Wilson cycle involved widespread tectono-metamorphic overprinting of crustal material along the western edge of BCS, as well as the (re-) assembly, rearrangement, and long-distance transport of various tectonic complexes that were thrust onto the hinterland of the BCS (e.g., Brueckner and van Roermund 2004, and references therein).

Fragments of the Caledonian-reworked BCS are currently exposed in tectonic windows along the axis of the orogen and in the western sector (Fig. 1). The largest and most intensely metamorphosed of these is the WGC. The

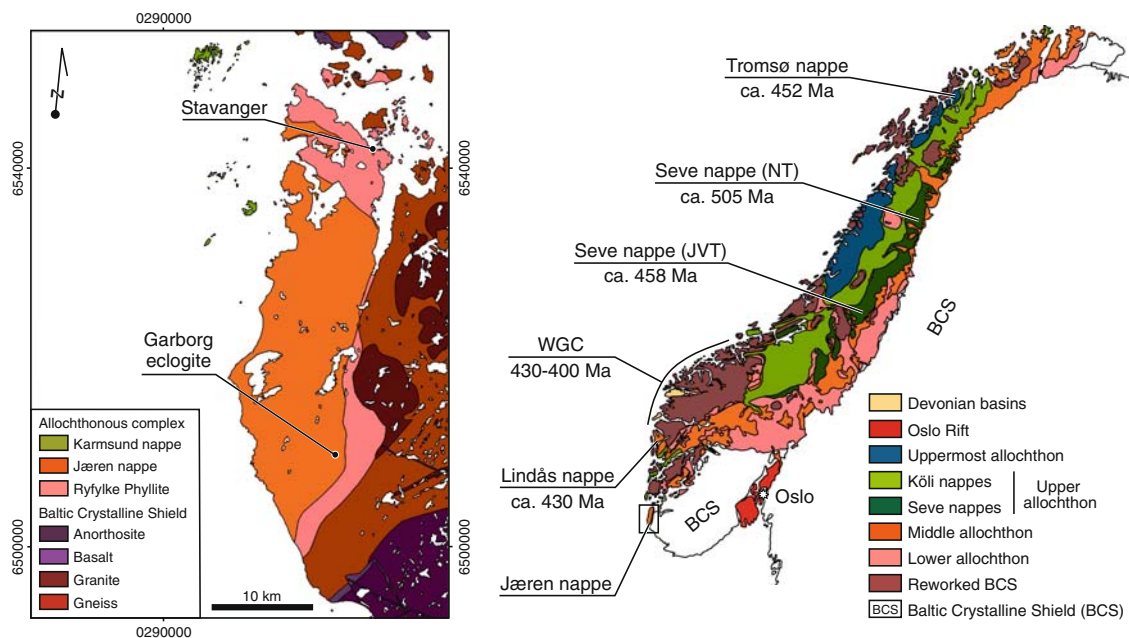


Fig. 1 Geological maps of the Jæren area based on Falkum (1982) and Majjer et al. (1987) and of the Scandinavian Caledonides modified after Roberts and Gee (1985) illustrating the position of the

Jæren area (box) and the other eclogite-bearing units with their estimated age of (U)HP metamorphism. Coordinates are in UTM and true north is indicated by the arrow

Caledonian deformation and metamorphism of this terrane becomes increasingly more pronounced and of higher grade towards the west and northwest (Krogh 1977; Griffin et al. 1985). In three regions on the west margin of the WGC—in the areas of Stadlandet–Nordfjord, Sørøyane, and Nordøyane–Moldefjord—the occurrence of coesite and diamond indicate that UHP metamorphic conditions were reached (e.g., Cuthbert et al. 2000). The (U)HP metamorphic overprint of WGC protoliths, which are of Sveconorwegian (=Grenvillian) or older age, documents long-lived, deep subduction of the Baltoscandian margin between 430 and 400 Ma (e.g., Kylander-Clark et al. 2009; Spengler et al. 2009).

Several tectonic units of the allochthonous complex that is juxtaposed between the WGC and the Baltic basement contain eclogite facies rocks (Fig. 1). The Lindås nappe of the Bergen Arcs consists of Sveconorwegian granulites (Bingen et al. 2001, 2004) that have been locally transformed to eclogite along veins and shear zones (Austheim 1987; Jamtveit et al. 1990). Eclogitization occurred at 1.8–2.1 GPa and ca. 700°C (Jamtveit et al. 1990), and has been dated at ca. 430 Ma using U–Pb zircon geochronology and Rb–Sr internal mineral isochrons (e.g., Kühn et al. 2002; Glodny et al. 2002; Bingen et al. 2004; Glodny et al. 2008b). The Seve Nappe Complex contains two main eclogite-bearing sub-units: the Norrbotten Terrane (NT; Andréasson et al. 1985) and the Jämtland–Västerbotten Terrane (JVT; Van Roermund 1985; Fig. 1). Despite apparent similarities in field occurrence and structural relationships, the eclogites from these areas yielded different peak metamorphic pressure estimates (1.5–2.7 GPa for the NT versus 1.4–1.8 GPa for the JVT; e.g., Brueckner and van Roermund 2004). Furthermore, HP metamorphism of the JVT occurred at 457.9 ± 4.5 Ma (weighted mean of 6 Sm–Nd ages by Brueckner and van Roermund 2007), i.e., significantly later than eclogitization of the Norrbotten eclogites (503.5 ± 9.2 Ma; weighted mean of three Sm–Nd ages by Mørk et al. 1988). Peak metamorphism of eclogites in the Tromsø nappe of northern Norway (Krogh et al. 1990) occurred at 2.8 GPa or possibly even higher pressure (Krogh-Ravna and Roux 2006) and was dated at 452.1 ± 1.7 Ma by U–Pb in eclogitic zircon (Corfu et al. 2003). Even though this age overlaps with the data reported for HP metamorphism of the JVT, the terranes are unrelated in terms of composition, affinity, and protolith age, and they occur in different tectono-stratigraphic levels of the orogenic thrust complex (Brueckner and van Roermund 2004, 2007).

This study focuses on the eclogites of the Jæren nappe, which is a tectonic subunit within the allochthonous thrust complex of SW Norway (Fig. 1). The nappe is sandwiched between the overlying Karmsund Nappe, which is dominated by ca. 490 Ma meta-ophiolites (Sturt and Thon 1978;

Dunning and Pedersen 1988), and a thin phyllite unit, which tectonically encloses slabs of Sveconorwegian gneiss (Roddick and Jorde 1981; Birkeland 1981). The three tectonic units together form the orogenic thrust complex in the Stavanger area. During the exhumation stage of the Scandian orogeny, this complex was emplaced onto the SW margin of the BCS (Verschure et al. 1980), which in this area mostly comprises felsic plutons and gneisses that yielded Sveconorwegian U–Pb zircon ages and provide evidence for 1.6- to 1.5-Ga age components (Möller et al. 2002). The basement rocks underwent ultrahigh temperature (UHT) metamorphism that was related to the ca. 930 Ma anorthosite emplacement (Schärer et al. 1996; Bingen and van Breemen 1998; Möller et al. 2002) and were pierced by ca. 616 Ma basaltic dikes (Bingen et al. 1998).

The Jæren nappe mainly consists of amphibolite facies gneisses, marbles, and quartzites. Locally, these rocks enclose kilometer-scale amphibolite and foliated granodiorite bodies (Birkeland 1981), the latter being of Sveconorwegian age (Roddick and Jorde 1981). The studied eclogites are exposed in the southeastern segment of the Jæren nappe, near the village of Garborg (Fig. 1). Only very limited geochronological data are available for these rocks. Polygenetic zircon grains in felsic lenses within the eclogites yielded a U–Pb age of ca. 920 Ma and contain a ca. 1,600 Ma age component (ID-TIMS analyses by Corfu, pers. comm.).

Field relationships and sample description

Outcrops in the study area are dominated by folded, mylonitized, and migmatized gneisses, comprising both amphibole- or mica-dominated rocks. These alternate on a decimeter- to decameter-scale and define a compositional banding structure that is parallel to the regional amphibolite-facies foliation. The eclogites occur either as bands that are concordant with the compositional layering in the host rocks or as decimeter- to decameter-sized lenses and boudins dispersed within the gneisses (Maijer et al. 1987, 1990; Smit et al. 2008). The eclogites are characterized by a HP foliation (S_1) that is defined by the alignment of fine-grained (<350 μm) omphacite and zoisite grains. In eclogite *bands*, the structure is sub-parallel or parallel to the compositional layering, therefore, to the regional amphibolite-facies foliation in the gneisses (S_2). The S_1 foliation in eclogite *lenses* is often at an angle to S_2 in the surrounding gneisses. Towards the retrogressed margins of the lenses, S_1 becomes gradually less pronounced and is overprinted by the S_2 structure.

The majority of the eclogites are mylonites that have a well-developed, penetrative S_1 fabric. In other eclogites,

the S_1 foliation shows a spacing of up to 5 mm and occurs between composite eclogitic microlithons characterized by a granular texture and grain sizes up to 2 mm. Based on textural and compositional characteristics, the eclogites were further subdivided into two types by Maijer et al. (1987). Type 1 eclogite is characterized by millimeter-scale, idioblastic garnet grains in a fine-grained ($<500\ \mu\text{m}$) foliated omphacite-, quartz-, and zoisite-rich matrix, whereas type 2 eclogite comprises millimeter-scale omphacite grains in a more-or-less foliated matrix of mostly zoisite, omphacite, garnet, quartz, and rutile. Eclogite boudins and lenses are dominated by type 2. Most eclogite bands consist of both type 1 and type 2, which alternate in a non-systematic way and are separated by ca. 10 cm thick transition zones of intermediate texture.

The eclogites comprise meta-basaltic rocks of E-MORB composition (Smit, unpublished data) that are dominated by the mineral assemblage garnet + omphacite + zoisite + clinozoisite + quartz + apatite + rutile \pm dolomite \pm kyanite \pm phengite \pm paragonite. Representative electron microprobe (EMPA) analyses were reported by Smit et al. (2008). Application of conventional geothermobarometry indicates pressure and temperature (P – T) conditions of 2.3–2.8 GPa and 585–655°C (Smit et al. 2008). Some eclogites have been subsequently affected by localized episodic CO_2 -metasomatism at equal or slightly lower pressures, giving rise to eclogite facies magnesite- and aragonite-bearing assemblages. Decompression was associated with an amphibolite facies deformational and metamorphic overprint, which caused the formation of the main mineral assemblages and deformation structures in the country-rock gneisses.

Six eclogite samples were selected for the current study. These include two type 1 (MS09001 and MS09002a) and two type 2 eclogites (MS08010 and MS08013b), as well as two eclogites of intermediate texture (MS03005 and MS10010d; for UTM coordinates see Supplementary Table 1). These samples were chosen because they cover the full range of observed eclogite textures and they are, with the exception of MS09002a, relatively pristine, meaning that over 80% of their volume consists of eclogite minerals. Simple outcrop maps of all sample locations are provided by Smit et al. (2008). Samples MS09001 and MS09002a (ca. 1 and 3 kg, respectively) are banded and foliated HP rocks from a single decimeter-thick eclogite layer. The layer is continuous over 2 meters, beyond which it is fragmented into a series of boudins. Similar rocks, which most likely represent the same layer, occur along strike in the same outcrop. Both samples contain relatively quartz-rich layers that host aragonite- and magnesite-bearing assemblages (Smit et al. 2008). These layers are separated from the bulk eclogite by a sharp interface in sample MS09001, whereas they define diffuse

compositional variations in sample MS09002a. In both samples, garnet is abundant (ca. 50 vol%) and relatively coarse-grained (up to 2.5 mm). Mineral inclusions in garnet mostly consist of omphacite, kyanite, zoisite, clinozoisite, phengite, dolomite, quartz, rutile, and fluorapatite. These phases are homogeneously distributed or concentrated in rings. The innermost 10–30 μm of some garnet grains host inclusions of taramitic amphibole, quartz, rutile, and ilmenite. Omphacite grains in the matrix (150–250 μm) and in pressure shadows of garnet (up to 2 mm) contain inclusions of rutile, quartz, garnet, and phengite. The matrix of MS09001 shows a well-developed S_1 fabric, whereas the retrogressed matrix of MS09002a is dominated by statically crystallized amphibole, secondary clinopyroxene, micas, and plagioclase. Samples MS08010 (ca. 6 kg) and MS08013b (ca. 8 kg) represent two partially retrogressed eclogite lenses. These samples only show the S_1 fabric. Both samples contain ca. 25 vol% of omphacite porphyroclasts (up to 2.3 mm) in a mylonitic matrix of omphacite, zoisite, clinozoisite, quartz, apatite, dolomite, rutile, and fine-grained ($<200\ \mu\text{m}$) garnet. The few inclusions that occur in omphacite and garnet consist of rutile and quartz, as well as other eclogite phases such as phengite and zoisite. The texturally intermediate sample MS03005 (ca. 2 kg) is from a transition zone between type 1 and 2 eclogites. The sample is a banded HP mylonite having an almost equigranular and relatively fine-grained (100–200 μm) eclogite assemblage. Inclusions in garnet and omphacite are common (up to 30 vol%) and mostly comprise rutile, garnet, and quartz. Sample MS10010d (ca. 4 kg) is from a meter-scale eclogite lens. The rock shows centimeter-scale compositional layering that reflects a variable modal abundance of quartz. Garnet grains (200–800 μm) contain sporadic inclusions of rutile, quartz, zoisite, and omphacite. These grains occur in a matrix that comprises (hyp-)idioblastic grains (150–250 μm) of omphacite, phengite, zoisite, and kyanite. The S_1 fabric in the sample is spaced and only weakly developed. The spatial distribution of S_1 structures is not related to variations in composition or garnet grain size.

Analytical methods

For whole-rock analysis, approximately 200 g of crushed sample were powdered in an agate ring mill. For mineral separation, the remaining crushed material was processed in a disk mill and was split into grain size fractions by sieving. Fractions containing monocrystalline garnet and omphacite grains were separated using a Frantz Isodynamic[®] magnetic separator. To avoid possible fractionation between core and rim based on differences in magnetic properties (Lapen et al. 2003), we carefully checked that

100% of the garnet and omphacite populations occurred within single magnetic fractions. The target phases were then handpicked under a binocular microscope. Clean, whole garnet grains or randomly picked grain fragments were selected for analysis (see representative photomicrographs in Supplementary Fig. 1). Care was taken to avoid fractionation based on color variations. Garnet grains hosting excessive amounts of inclusions were excluded, because these may harbor assemblages that crystallized during retrograde fracturing. In case of samples MS09001 and MS09002a, garnet fragments were sorted into different fractions by sieve size. Sample MS09002a allowed handpicking of whole garnet grains. The different separates were analyzed to test the influence of garnet grain size on ages and to monitor possible effects of analyzing whole garnet grains versus grain fragments.

Unlike garnet color, which can vary from core to rim depending on composition, omphacite color is typically uniform throughout grains. In the case of samples in which omphacite was partially replaced in a pseudomorphic fashion by amphibole, omphacite-bearing size fractions comprise grains having similar crystal shape and magnetic properties, but a different green color. To unambiguously identify omphacite in these fractions, different grains representing the variable tones of green in each sample were analyzed by confocal micro-Raman spectroscopy using the Jobin–Yvon HR-800 dispersive Raman spectrometer (for analytical details see Smit et al. 2008). The analyses showed that the green tone of omphacite varied from sample to sample and that a green tone typical of omphacite in one sample represented amphibole in another. It is stressed here that for accurate geochronological analysis of omphacite, the phase must be unambiguously separated from retrograde minerals. In cases where optical identification is difficult, the application of spectroscopic techniques is helpful. After the Raman identification test, omphacite grains were hand picked under a binocular microscope. Selected omphacite grains represent either the porphyroblastic assemblage that defines the S_1 (MS03005, MS09001, and MS10010d) or fragments of a coarse-grained, porphyroclastic omphacite population (MS08010 and MS08013b). Photomicrographs of omphacite separates are shown in Supplementary Fig. 1.

For EPMA and laser ablation ICP-MS (LA-ICP-MS) studies, omphacite and whole garnet grains were mounted in epoxy and polished down to their approximate geometric centers. The garnet grains were subjected to X-ray mapping by use of a JEOL JXA-8900M Superprobe[®]. The Ca X-ray maps of the grains that were used for modeling are shown in Fig. 2a, d and Supplementary Fig. 2a. Unmarked Ca maps and maps of the Fe-, Mg-, and Mn-content of these grains are included in Supplementary Fig. 3. Trace element analysis was performed by LA-ICP-MS using a New Wave

Research UP193HE ArF Excimer laser ablation system ($\lambda = 193$ nm), operating with ca. 9 J/cm² at 5 Hz, coupled to a Thermo Scientific[®] Element2 ICP-MS. After 40 s of baseline monitoring, grains were analyzed for 1 min using a spot diameter of 25–35 μ m for garnet and 90 μ m for omphacite. During this period, 32 sweeps through the targeted isotope spectrum were performed. The Si contents based on EPMA data were used as an internal standard. External standardization was done by performing two replicate measurements of the NIST SRM-612 glass standard (Pearce et al. 1997; Jochum et al. 2005) between every 5 unknowns. Standards were crosschecked for accuracy by measuring the USGS BHVO-2G glass as an unknown. The accepted values for this standard (Jochum et al. 2005) lie within error (i.e., 2 SD) of the average concentration determined for each element. Data were screened and were filtered for inclusions by using isotope monitors (e.g., ⁴³Ca, ⁴⁹Ti, ⁸⁸Sr, ⁹⁰Zr). Precision on rare-earth element (REE) concentrations (based on measurements of the isotopes ¹³⁹La, ¹⁴⁰Ce, ¹⁴¹Pr, ¹⁴⁶Nd, ¹⁴⁷Sm, ¹⁵³Eu, ¹⁵⁷Gd, ¹⁵⁹Tb, ¹⁶³Dy, ¹⁶⁵Ho, ¹⁶⁶Er, ¹⁶⁹Tm, ¹⁷²Yb, and ¹⁷⁵Lu) is 6–20% (1 SD) depending on absolute elemental abundance. Precision on V and Y concentrations (measured using ⁵¹V and ⁸⁹Y, respectively) is better than 8%. Detection limits for the analyses of REE, V, and Y were below 0.3, 0.5, and 0.1 ppm, respectively. Results are summarized in Figs. 2, 3 and Supplementary Figs. 2, 4.

For Lu–Hf and Sm–Nd studies, mineral separates were cleaned in 2.5 M HCl at room temperature and were rinsed with de-ionized water. Garnet and omphacite fractions, as well as whole-rock samples were spiked with mixed ¹⁷⁶Lu–¹⁸⁰Hf and ¹⁴⁹Sm–¹⁵⁰Nd isotope tracers. Garnet and omphacite fractions were digested in Savillex screw-top PFA vials by sequential addition of HF–HNO₃–HClO₄ (4:2:1) and 10 M HCl, both steps being followed by drying down on a hot plate. This process was repeated until addition of the HCl provided a clear solution, indicating that full digestion of the target phase was achieved. This method dissolves the target phases while leaving behind robust phases that potentially harbor inherited Hf isotope signatures (e.g., rutile and zircon). Whole rock powders were digested in closed Savillex vials with HF–HNO₃ on a hot plate and were then evaporated to dryness. After adding more HF–HNO₃ to the vials, they were closed and placed with a few ml H₂O into steel-jacketed Teflon[®] bombs at 180°C for 5 days to complete the digestion of refractory phases. All digested samples were then dried down again and were dissolved in 6 M HCl, then diluted to 3 M HCl with H₂O, and centrifuged. The spike-equilibrated solutions were then loaded onto heat-shrink Teflon[®] columns containing Eichrom[®] Ln-Spec resin, where Lu and Hf were separated from the matrix elements using the method of Münker et al. (2001). The Lu and Hf fractions were

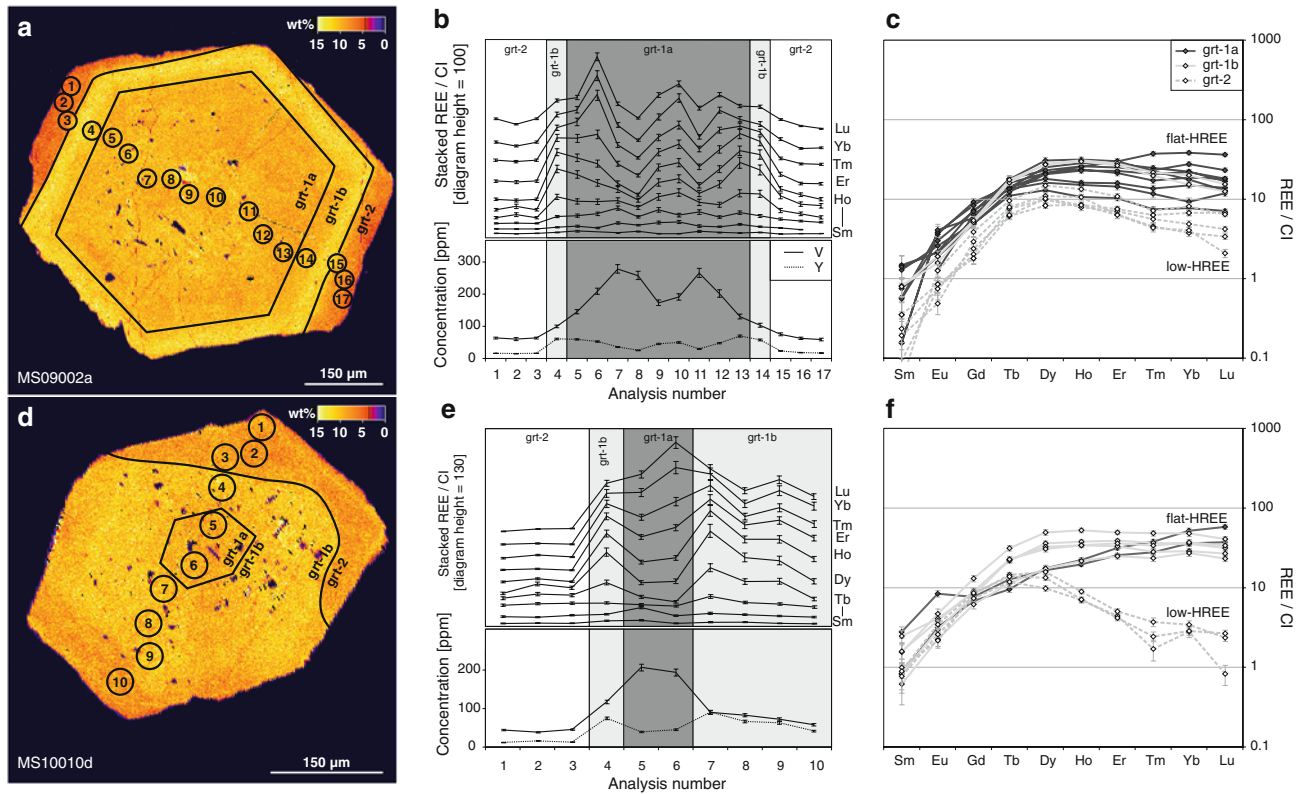


Fig. 2 Composition of representative garnet grains from samples MS09002a (a–c) and MS10010d (d–f), which were selected for age modeling: **a, d** X-ray maps for Ca showing the spatial distribution of the transition between individual garnet zones (solid black lines, unmarked Ca maps are shown in Supplementary Fig. 3) and the spots measured by LA-ICP-MS; **b, e** V, Y, and stacked REE profiles. In grt-

1a zones, the V profile is mirrored by that of Y, which is similar to M- to HREE profiles (e.g., that of Ho); **c, f** CI-chondrite-normalized REE diagrams (CI-chondrite values after Boynton 1984). The results for the other samples (MS03005, MS08010, MS08013b, and MS09001) are compiled in the Supplementary Fig. 2, whereas enlargements of the Lu and Sm profiles can be found in Supplementary Fig. 6

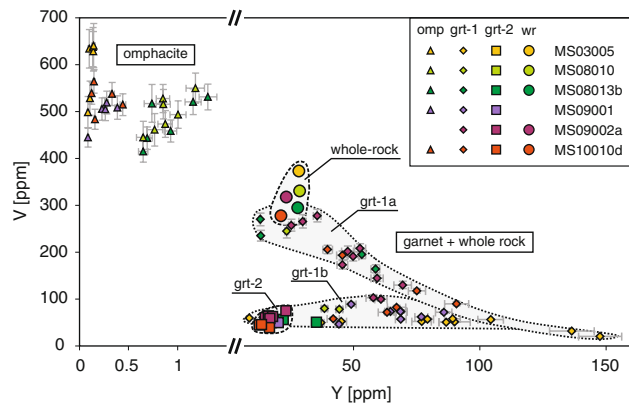


Fig. 3 V versus Y diagram showing the abundance of these trace elements in omphacite ('omp'), in grt-1a, grt-1b, and grt-2 zones, and in whole-rocks ('wr', Smit, unpublished data). Analyses of different garnet zones are highlighted. No omphacite was available for sample MS09002a and no whole rock analysis was performed for MS09001

purified further by passing them separately through the same columns, but using an abbreviated elution procedure and loading in HCl and ascorbic acid so that Fe is eluted

rapidly as Fe^{2+} (P. Sprung, pers. comm.). The matrix cut from the first stage, which contains the light- and middle REE (LREE and MREE), was loaded in 2.5 M HCl onto glass columns containing Bio-Rad[®] 50 W-X8 resin. A REE cut was separated using 2.5 and 6 M HCl as eluents and was subsequently loaded onto glass columns packed with Teflon[®] beads coated with di-(2-ethyl-hexyl) phosphoric acid (HDEHP). Separation of Nd and Sm from the other REE and from each other was achieved by using 0.17 M and 0.4 M HCl, respectively.

Isotope analysis was done using a Micromass IsoProbe[®] MC-ICP-MS. The Hf standard used in this study is made from AMES Hf metal and has an isotope composition that is indistinguishable from that of the international JMC-475 standard. Hafnium and neodymium isotope ratios were corrected for mass bias using the exponential law and $^{179}\text{Hf}/^{177}\text{Hf} = 0.7325$ and $^{146}\text{Nd}/^{144}\text{Nd} = 0.7219$, respectively. The resulting $^{176}\text{Hf}/^{177}\text{Hf}$ values are reported relative to the JMC-475 value of 0.282163, whereas the $^{143}\text{Nd}/^{144}\text{Nd}$ measurements are reported relative to 0.511858 for the La Jolla Nd standard. The external

reproducibilities of $^{176}\text{Hf}/^{177}\text{Hf}$ and $^{143}\text{Nd}/^{144}\text{Nd}$ analyses were estimated for individual analysis sessions by measuring standard solutions at various concentrations that spanned those of the sample solutions (8, 24, 40, and 80 ppb; see Bizzarro et al. 2003). In general, the external reproducibility (% 2 SD of multiple analyses of a single solution) is about twice the internal run statistic (% 2 SE of individual analyses). Instrumental drift, if present, was monitored by running standards after every 4–6 samples. Isochron ages and uncertainties were calculated using Isoplot v. 3.27 (Ludwig 2005) and decay constants of $1.867 \times 10^{-11} \text{ year}^{-1}$ for ^{176}Lu (Scherer et al. 2001, 2003; Söderlund et al. 2004) and $6.54 \times 10^{-12} \text{ year}^{-1}$ for ^{147}Sm . The Lu–Hf and Sm–Nd data, and associated ages are compiled in Table 1. Isochron plots for the Lu–Hf and Sm–Nd data are presented in Figs. 4, 5, and Supplementary Fig. 5. Uncertainties on calculated ages and initial isotope compositions are reported at the 2 SD-level, whereas the 95% confidence limits are quoted for weighted means and errors on intercepts. The uncertainties in the ^{176}Lu and ^{147}Sm decay constants are approximately 0.6 and 1.5%, respectively (Begemann et al. 2001, 2001; Scherer et al. 2001, 2003; Söderlund et al. 2004). For the purpose of comparing ages derived from a single isotope system, decay constant uncertainties have not been propagated into the ages.

Results

Garnet and omphacite trace element composition

Garnet grains are dominated by a central domain that is characterized by (1) concentric small-scale variations in Ca concentration with an overall increase in Ca from core to rim, (2) more-or-less obscured concentric variations in Fe and Mg concentrations, which are inversely related, and (3) Mn distributions that are often smoothed equivalents of the Fe distribution (Fig. 2, Supplementary Figs. 2a, 3). Such garnet zones are referred to as grt-1. With the exception of MS03005, garnet grains from all analyzed samples are rimmed by low-grossular garnet (grt-2), which occurs either as concordant rims (e.g., Fig. 2a) or as irregularly shaped zones (e.g., Fig. 2d). With the exception of blue-amphibole-bearing assemblages in the cores of some grains, the abundant inclusions in grt-1 comprise eclogite minerals. No inclusions were identified in grt-2 rims.

The distribution of REE in grt-1 domains is generally symmetric (Fig. 2, Supplementary Fig. 2b). Peak concentrations of the different REE occur at variable distance from the geometric cores of grains. Changes in the heavy REE (HREE) content within grt-1 zones are relatively abrupt, resulting in two types of REE patterns: one that is

relatively flat with respect to the HREE normalized to CI-chondrite (hereafter ‘flat-HREE’) and another that is characterized by a decreasing concentration of HREE with increasing atomic number (‘low-HREE’, Fig. 2, Supplementary Fig. 2c). The grt-2 zones show relatively homogeneous REE content and yield only low-HREE patterns. The shift in REE composition along the interface between grt-1 and grt-2 is as abrupt as the change in Ca composition.

Garnet REE zoning is controlled by many aspects such as reactions that occur during garnet growth (e.g., Hickmott et al. 1987; Konrad-Schmolke et al. 2009), the fractionation of these elements into garnet relative to the matrix (e.g., Otamendi et al. 2002; Lapen et al. 2003; Kohn 2009), and rates at which they diffuse through the matrix towards the garnet surface (Skora et al. 2006; Kohn 2009) and through a garnet volume (Van Orman et al. 2002; Tirone et al. 2005). Identification of the imprint of metamorphic processes on garnet REE zoning requires knowledge on whether their incorporation into garnet was limited by diffusion through the matrix. This may be attained through a careful evaluation of the spatial distribution of REE relative to elements that fractionate equally or less strongly into garnet relative to the matrix and which diffuse faster through the rock matrix. For this purpose, we have compared zoning of Y and V in garnet. Yttrium is chemically similar to the middle- to heavier REE (e.g., Ho; Fig. 2), but is usually more abundant in the studied phases and could therefore be measured more precisely; hence it is used here as a M- to HREE proxy. Vanadium (as V^{3+}) generally partitions less strongly into garnet than Y (e.g., data of Hermann 2002). Considering that matrix diffusion coefficients at least partly depend on ionic radius (IR), V (IR = 0.064 nm; Shannon 1976) is assumed to diffuse faster to the surface of growing garnet crystals than Y (IR = 0.090 nm; Shannon 1976).

The abundances of V and Y vary significantly across grt-1 zones. The abundances co-vary in central grt-1 zones (grt-1a) and, from core to rim, trend initially towards and then away from the whole-rock composition in Fig. 3. The change from increasing to decreasing V content from the core outwards in MS09002a is associated with a drastic decrease in the abundance of M- and HREE, forming low-HREE patterns. The abundance of V in grt-1a zones from MS03005 garnet is relatively low and shows only minor variation, plotting on the lower extent of the grt-1a trend. In mantles of grt-1 (grt-1b), Y shows core-to-rim depletion at relatively constant or steadily decreasing V content. The abundance of V and Y throughout grt-1b zones trends towards the composition of grt-2, which is relatively homogeneous among and between eclogite samples (Fig. 3). Although the V content of grt-1a zones of garnet in MS03005 is relatively low and is lower than that of

Table 1 Lu–Hf and Sm–Nd isotope data for HP rocks from the Garborg area

Sample fraction	Grain size (μm)	Lu (ppm)	Hf (ppm)	$^{176}\text{Lu}/^{177}\text{Hf}$	$^{176}\text{Hf}/^{177}\text{Hf}$	Lu–Hf age (Ma)	Sm (ppm)	Nd (ppm)	$^{147}\text{Sm}/^{144}\text{Nd}$	$^{143}\text{Nd}/^{144}\text{Nd}$	Sm–Nd age (Ma)
MS03005											
grt.A.1	180–250	1.51	0.357	0.6027 \pm 15	0.287939 \pm 30		0.207	0.0864	1.449 \pm 4	0.51638 \pm 21	
grt.B.1	180–250	1.55	0.541	0.4076 \pm 10	0.286255 \pm 16		–	–	–	–	
grt.B.2	180–250	1.64	0.642	0.3627 \pm 9	0.285903 \pm 19		–	–	–	–	
grt.B.3	180–250	1.55	0.658	0.3338 \pm 8	0.285636 \pm 20		–	–	–	–	
grt.B.1–3 ^a	180–250	–	–	–	–		0.210	0.0770	1.653 \pm 4	0.51692 \pm 15	
omp.A.1	180–250	0.051	0.234	0.009161 \pm 70	0.28290 \pm 27		–	–	–	–	
omp.B.1	180–250	0.0113	0.247	0.006768 \pm 27	0.282831 \pm 46		0.414	1.22	0.2058 \pm 5	0.512825 \pm 48	
wr.A.1	–	0.473	2.14	0.03137 \pm 8	0.283035 \pm 15		3.40	12.1	0.1703 \pm 4	0.512743 \pm 16	431 \pm 13
MS08010											
grt.A.1	180–250	0.824	0.163	0.7163 \pm 18	0.289084 \pm 82		0.353	0.179	1.192 \pm 3	0.51586 \pm 16	
grt.B.1	180–250	0.954	0.317	0.4277 \pm 11	0.286624 \pm 27		0.411	0.304	0.8182 \pm 20	0.514719 \pm 90	
grt.B.2	180–250	0.961	0.291	0.4697 \pm 12	0.286908 \pm 33		0.391	0.231	1.024 \pm 3	0.51534 \pm 11	
omp.A.1	250–355	–	–	–	–		0.314	0.632	0.3005 \pm 8	0.51315 \pm 15	
omp.B.1	250–355	0.0266	0.224	0.01684 \pm 4	0.282954 \pm 32		0.260	0.388	0.4060 \pm 10	0.513447 \pm 69	
wr.A.1	–	0.512	1.65	0.04413 \pm 12	0.283152 \pm 17		0.997	2.73	0.2208 \pm 6	0.512910 \pm 22	462 \pm 14
MS08013b											
grt.A.1	180–250	1.07	0.0891	1.705 \pm 4	0.29782 \pm 18		–	–	–	–	
grt.B.1	180–250	1.00	0.166	0.8571 \pm 21	0.290360 \pm 32		0.144	0.0679	1.280 \pm 3	0.51635 \pm 22	
grt.B.2	180–250	1.01	0.138	1.035 \pm 3	0.291871 \pm 43		0.152	0.0805	1.141 \pm 3	0.51573 \pm 17	
omp.A.1	250–355	0.00889	0.236	0.005344 \pm 15	0.282862 \pm 35		0.165	0.391	0.2546 \pm 6	0.513089 \pm 62	
wr.A.1	–	0.468	1.50	0.04420 \pm 12	0.283164 \pm 17		3.53	10.2	0.2087 \pm 5	0.512971 \pm 16	464 \pm 20
MS09001											
grt.A.1	355–500	2.01	0.133	2.163 \pm 5	0.301959 \pm 15		0.181	0.111	0.9852 \pm 25	0.515241 \pm 99	
grt.A.2	355–500	1.78	0.158	1.609 \pm 4	0.296996 \pm 29		0.175	0.102	1.034 \pm 3	0.51549 \pm 13	
grt.A.3	355–500	2.03	0.226	1.276 \pm 3	0.294091 \pm 29		0.190	0.132	0.8677 \pm 22	0.51500 \pm 11	
grt.B.1	250–355	1.85	0.150	1.755 \pm 4	0.298317 \pm 22		0.163	0.0549	1.801 \pm 5	0.51772 \pm 15	
omp.A.1	180–250	0.0850	0.207	0.05836 \pm 16	0.28313 \pm 36		0.463	1.55	0.1803 \pm 5	0.512890 \pm 85	
omp.B.1	180–250	–	–	–	–		0.412	1.31	0.1902 \pm 5	0.512941 \pm 46	
wr.A.1	–	0.322	1.48	0.03101 \pm 8	0.283108 \pm 18		2.24	7.27	0.1866 \pm 5	0.512929 \pm 20	453.4 \pm 9.6

Table 1 continued

Sample fraction	Grain size (μm)	Lu (ppm)	Hf (ppm)	$^{176}\text{Lu}/^{177}\text{Hf}$	$^{176}\text{Hf}/^{177}\text{Hf}$	Lu–Hf age (Ma)	Sm (ppm)	Nd (ppm)	$^{147}\text{Sm}/^{144}\text{Nd}$	$^{143}\text{Nd}/^{144}\text{Nd}$	Sm–Nd age (Ma)
MS09002a											
grt.A.1 ^b	500–750	0.927	0.244	0.5421 \pm 14	0.287601 \pm 17		0.179	0.213	0.5084 \pm 13	0.513892 \pm 76	
grt.A.2	500–750	1.97	0.185	1.518 \pm 4	0.296166 \pm 18		0.182	0.121	0.9124 \pm 22	0.515177 \pm 79	
grt.A.3	500–750	2.04	0.160	1.820 \pm 5	0.298865 \pm 22		0.175	0.106	0.9987 \pm 24	0.515355 \pm 99	
grt.B.1 ^b	355–500	1.03	0.353	0.4155 \pm 11	0.286487 \pm 18		0.172	0.194	0.5362 \pm 13	0.51398 \pm 10	
grt.B.2	355–500	2.15	0.208	1.470 \pm 4	0.295799 \pm 18		0.157	0.0621	1.530 \pm 4	0.51706 \pm 14	
grt.B.3	355–500	2.14	0.157	1.947 \pm 5	0.299989 \pm 19		0.163	0.0675	1.466 \pm 4	0.51685 \pm 14	
wr.A.1	–	0.373	1.52	0.03498 \pm 9	0.283150 \pm 14	469.3 \pm 0.8	2.24	6.88	0.1791 \pm 5	0.512882 \pm 15	470.7 \pm 8.3
MS10010d											
grt.A.1	250–355	1.11	0.145	1.088 \pm 3	0.292424 \pm 11		0.242	0.0776	1.890 \pm 5	0.51800 \pm 10	
grt.B.1	250–355	1.06	0.234	0.6429 \pm 16	0.288492 \pm 25		0.245	0.0851	1.741 \pm 4	0.51761 \pm 14	
grt.B.2	250–355	1.07	0.288	0.5281 \pm 13	0.287463 \pm 16		0.258	0.101	1.548 \pm 4	0.516989 \pm 91	
omp.A.1	180–250	0.0181	0.200	0.01281 \pm 4	0.28285 \pm 24		–	–	–	–	
omp.B.1	180–250	0.00742	0.216	0.004876 \pm 15	0.282839 \pm 52		0.472	0.712	0.4011 \pm 10	0.513551 \pm 65	
wr.A.1	–	0.330	1.28	0.03672 \pm 10	0.283142 \pm 17	470.7 \pm 1.5	1.57	5.06	0.1880 \pm 5	0.512914 \pm 16	457.7 \pm 6.2

Uncertainties on isotope ratios are 2 SD in the least significant digits. Fraction names include an abbreviation for the phase (grt = garnet, omp = omphacite, wr = whole rock), a letter for the mineral or whole rock separate, and a number for the fraction of each separate. Analyses in italics were excluded from isochron regressions (see text)

^a Mixed aliquot of the samples grt.B.1–3

^b Whole grains only

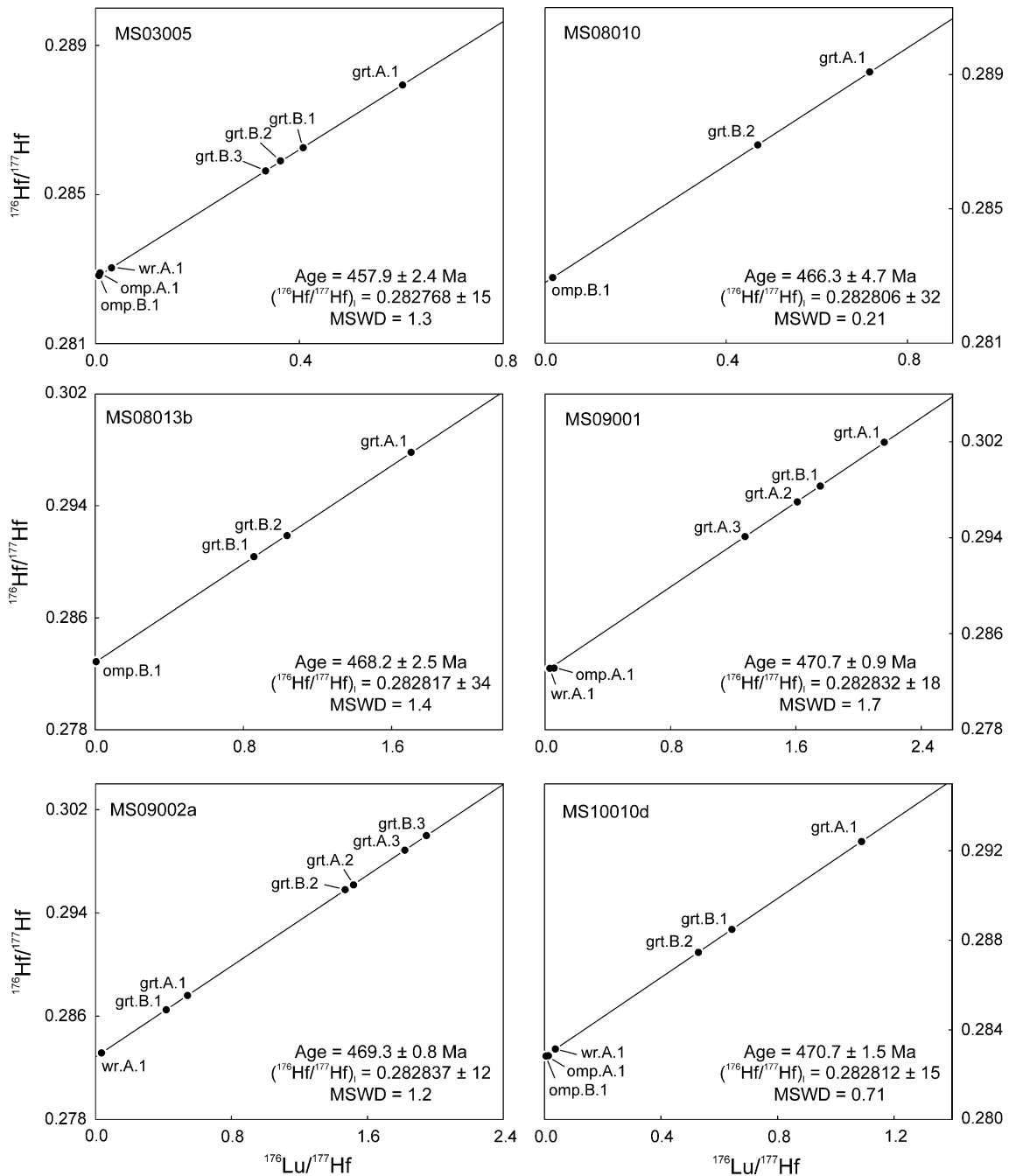


Fig. 4 Lu–Hf isochrons for the studied samples

grt-1b in the same sample, grt-1a compositions for this sample plot on the typical grt-1a trend in Fig. 3.

In the context of interpreting Lu–Hf and Sm–Nd age data, the Lu- and Sm contributions of individual garnet zones relative to the bulk-garnet Lu and Sm (X'_{Lu} and X'_{Sm}) were modeled following the methods and assumptions listed in Supplementary Text 1 and using the LA-ICP-MS data of representative garnet grains as input (Supplementary Table 2). The results, assuming a 10% 2 SD

uncertainty on X' due to variability of Lu- and Sm concentration and the relative volume of garnet zones among eclogite samples, are provided in Table 2 and Supplementary Fig. 6. For samples that have grt-2 zones, the relative contribution of Lu by these zones to the bulk-garnet Lu ($X'_{\text{Lu}}^{\text{grt-2}}$) varies between 0.02 and 0.28. The complementary Lu is provided by grt-1a and grt-1b. The relative contribution by either of these grt-1 zones varies strongly ($\Delta X'_{\text{Lu}} > 0.60$). Due to relatively higher

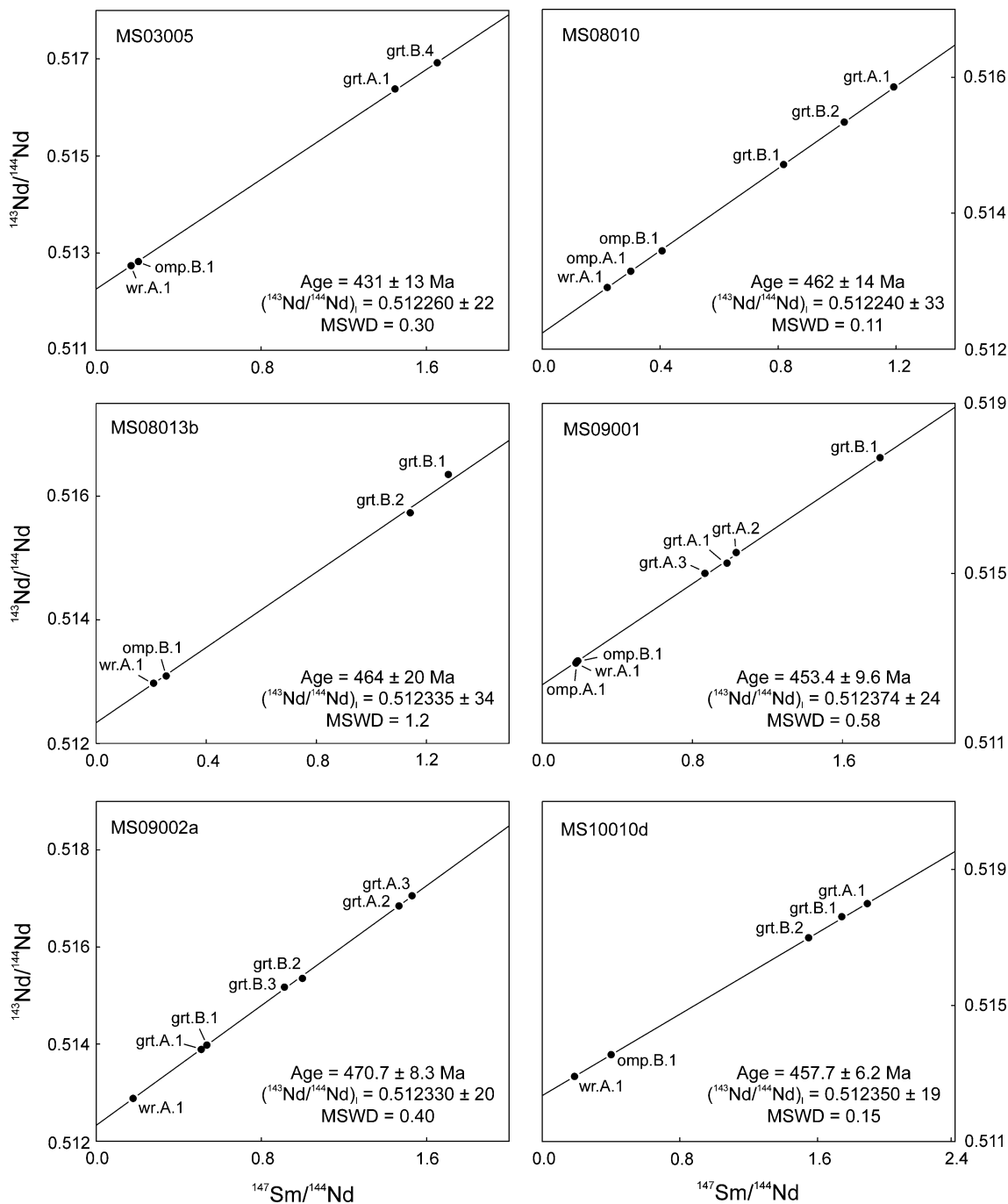


Fig. 5 Sm–Nd isochrons for the studied samples

abundance of Sm in grt-2 zones, $X_{\text{Sm}}^{\text{grt-2}}$ is generally higher than $X_{\text{Lu}}^{\text{grt-2}}$ and ranges from 0.07 to 0.53. For both Lu and Sm, there is no correlation between $X^{\text{grt-1a}}$ or $X^{\text{grt-1b}}$, and $X^{\text{grt-2}}$.

The chondrite-normalized REE content in omphacite typically increases with increasing atomic number for the LREE, reaches a maximum in the MREE range, and decreases for the HREE (Supplementary Fig. 4). Differences

between samples in the absolute REE abundance of omphacite, and in the slopes and the position of the peak in the CI-normalized REE diagram relate to differences in whole-rock REE content. Abundances of V vary between 415 and 640 ppm and they show a weak positive correlation with Y contents, which are relatively low (<2 ppm, Fig. 3). Compositional variations within samples are relatively small and not resolvable within individual grains.

Table 2 The modeled relative contribution of Lu and Sm of grt-1a, grt-1b, and grt-2 zones to the bulk-garnet Lu and Sm

Sample	X'_{Lu}^{grt-1a}	X'_{Lu}^{grt-1b}	X'_{Lu}^{grt-2}	X'_{Sm}^{grt-1a}	X'_{Sm}^{grt-1b}	X'_{Sm}^{grt-2}
MS03005	0.58 ± 0.03	0.42 ± 0.03	–	0.09 ± 0.05	0.91 ± 0.05	–
MS08010	0.07 ± 0.04	0.64 ± 0.04	0.28 ± 0.03	0.04 ± 0.02	0.43 ± 0.02	0.53 ± 0.03
MS08013b	0.53 ± 0.02	0.26 ± 0.02	0.21 ± 0.04	0.77 ± 0.04	0.12 ± 0.04	0.11 ± 0.05
MS09001	0.00 ± 0.00	0.98 ± 0.00	0.02 ± 0.02	0.00 ± 0.00	0.87 ± 0.00	0.13 ± 0.05
MS09002a	0.61 ± 0.03	0.29 ± 0.03	0.10 ± 0.05	0.66 ± 0.03	0.27 ± 0.03	0.07 ± 0.05
MS10010d	0.25 ± 0.03	0.72 ± 0.03	0.03 ± 0.03	0.21 ± 0.03	0.57 ± 0.03	0.22 ± 0.03

Geochronology

Lu–Hf

Lutetium–Hafnium geochronology provided six high-precision internal isochrons (Fig. 4; Table 1). Sample MS03005 yielded a 7-point garnet + omphacite + whole-rock isochron with an age of 457.9 ± 2.4 Ma (MSWD = 1.3). A mineral isochron for sample MS08010, including all garnet analyses, indicates an age of 470 ± 27 (MSWD = 8.1). Excluding the grt.B.1 analysis significantly improves isochron statistics (466.3 ± 4.7 Ma, MSWD = 0.21) without significantly changing the age. The mineral isochron for MS08013b provides an age of 468.2 ± 2.5 Ma (MSWD = 1.4). Including the whole-rock analyses for both MS08010 and MS08013b provides identical, but relatively imprecise ages of 469 ± 14 Ma (MSWD = 2.7) and 470.0 ± 4.9 Ma (MSWD = 2.6), respectively. Sample MS09001 yielded a garnet + omphacite + whole-rock isochron age of 470.7 ± 0.9 (MSWD = 1.7). The isochron for sample MS09002a, which is based on one whole rock and six garnet analyses, yields 469.3 ± 0.8 Ma (MSWD = 1.2). The Lu–Hf age of the 6-point garnet + omphacite + whole-rock isochron for sample MS10010d is 470.7 ± 1.5 (MSWD = 0.71). For all samples except MS03005, the isochron ages overlap within 2 SD and provide a weighted mean age of 469.9 ± 1.2 Ma. For the five samples that have overlapping Lu–Hf ages, the calculated initial $^{176}\text{Hf}/^{177}\text{Hf}$ values also overlap within 2 SD, giving a weighted mean of 0.282826 ± 0.000017 . The calculated initial $^{176}\text{Hf}/^{177}\text{Hf}$ values for sample MS03005 is significantly lower (0.282768 ± 0.000015). The whole-rock analyses by themselves do not define a Lu–Hf isochron. Calculation of depleted-mantle model-ages (t_{DM}) using the CHUR parameters of Bouvier et al. (2008) yielded no solution for the type 2 samples MS08010 and MS08013b and gave highly variable results between 850 and 1,760 Ma for the other samples. The present day ϵ_{Hf} value for sample MS03005 (+8.8) is lower than those of the other samples (+11.4 to +13.4).

The duration of garnet growth may exceed our chronological resolution, either due to slow growth rates or due to polygenesis. In such cases, the bulk garnet Lu–Hf and Sm–Nd ages would represent the average age of all growth zones weighted by their respective Lu and Sm contents (Lapen et al. 2003; Kohn 2009). To enable interpretation of the Lu–Hf ages, possible relationships between these ages and the distribution of Lu, i.e., the modeled Lu contribution of different garnet growth zones to the bulk garnet Lu (X'_{Lu}), were evaluated. A strong correlation exists between X'_{Lu}^{grt-2} and Lu–Hf isochron age. A linear regression through the data ($R^2 = 0.97$) allows the estimation of intercepts at 471.0 ± 0.9 Ma for $X'_{Lu}^{grt-2} = 0$ and 455 ± 10 for $X'_{Lu}^{grt-2} = 1$ (Fig. 6a). The older intercept at $X'_{Lu}^{grt-2} = 0$ is taken as an estimate of the grt-1 age, whereas the younger intercept at $X'_{Lu}^{grt-2} = 1$ provides an estimate of the grt-2 age. If the grt-2 age component is removed by projecting it through the data points back to $X'_{Lu}^{grt-2} = 0$, it is then possible to evaluate any age difference between grt-1a and grt-1b zones by the same approach. There is no significant correlation ($R^2 = 0.11$) between the resulting grt-1 age estimates and the distribution of Lu between grt-1a and grt-1b (Fig. 6b).

Sm–Nd

The results of Sm–Nd geochronology are shown in Fig. 5 and Table 1. Sample MS03005 provided the youngest isochron age (431 ± 13 Ma, MSWD = 0.30). Samples MS09001 and MS10010d yielded slightly older ages of 453.4 ± 9.6 Ma (MSWD = 0.58) and 457.7 ± 6.2 Ma (MSWD = 0.15), respectively. The isochrons for samples MS08010 and MS08013b indicate ages of 462 ± 14 Ma (MSWD = 0.11) and 464 ± 20 Ma (MSWD = 1.2), respectively. These apparent ages overlap within their relatively large uncertainties with the weighted mean of the Lu–Hf age cluster (469.9 ± 1.2 Ma). The garnet + whole-rock isochron of sample MS09002a provided an age of 470.7 ± 8.3 Ma (MSWD = 0.40). Calculated initial $^{143}\text{Nd}/^{144}\text{Nd}$ values range from 0.512240 to 0.512374, providing a weighted mean of 0.512322 ± 0.000051 . No

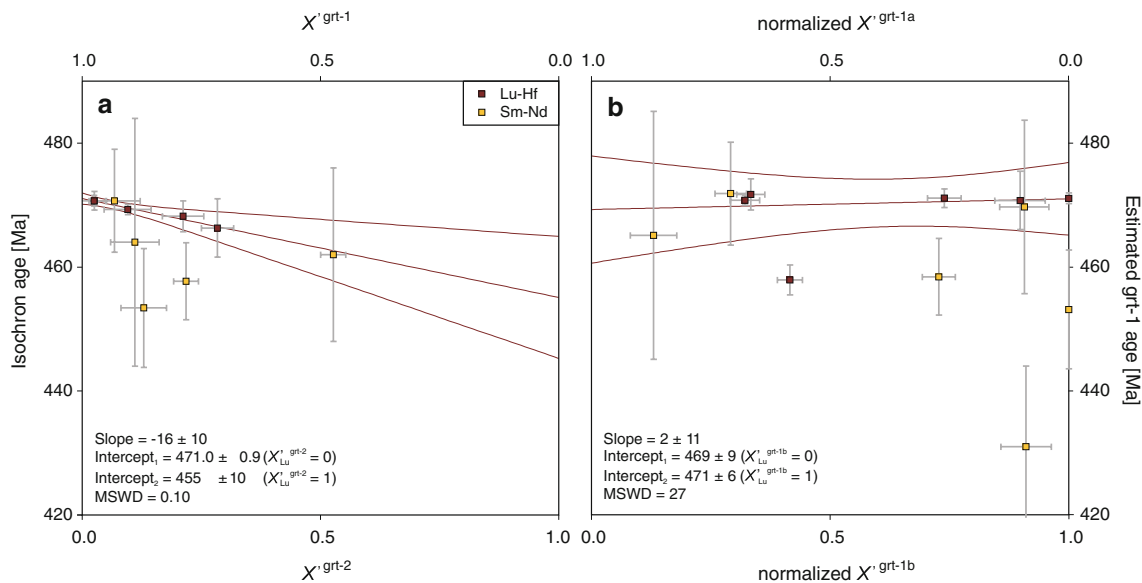


Fig. 6 Relationship between isochron age and the relative contributions of Lu and Sm by individual garnet zones to the bulk garnet Lu and Sm for the studied samples: **a** isochron age versus $X^{\text{grt-2}}$ ($= 1 - X^{\text{grt-1}}$) for Lu and Sm for samples that contain grt-2 zones, i.e., all samples except MS03005; **b** estimated grt-1 age versus the relative Lu and Sm contribution by grt-1a and -1b ($X^{\text{grt-1a}}$ and $X^{\text{grt-1b}}$) for all

statistically valid Sm–Nd isochron could be constructed from whole-rock isotope data. Calculation of t_{DM} using the CHUR values of Bouvier et al. (2008) did not yield systematic results. The present-day ε_{Nd} value for sample MS03005 is +2.2, whereas other samples provide more positive values (+4.9 to +6.6). The Sm–Nd age data fall on or below the regression line through Lu–Hf age vs. $X_{\text{Lu}}^{\text{grt-2}}$ (Fig. 6a). As was the case for Lu, there is no significant correlation ($R^2 = 0.37$) between grt-1 age estimates and the distribution of grt-1 Sm between grt-1a and grt-1b (Fig. 6b).

Discussion

Linking garnet compositions to petrological processes

Spatial distribution patterns of REE and other trace elements are potentially important indicators for the process that operated during garnet growth (e.g., Hickmott et al. 1987). Co-varying elemental contents from core to rim may be diagnostic of specific reactions such as amphibole- or epidote breakdown (Konrad-Schmolke et al. 2009). However, different elements may be released into—or taken up from—the matrix during a wide variety of mineral reactions that are not necessarily coeval (e.g., the breakdown of titanite, amphibole, or epidote, or the crystallization of zoisite and rutile), making trace element compositional variations difficult to interpret in terms of reaction

studied samples (including MS03005). The grt-1 age is estimated by projecting the estimated grt-2 age (455 ± 10 Ma) through the data points in the isochron age versus $X^{\text{grt-2}}$ plot (a) to $X^{\text{grt-2}} = 0$. Regression lines are based on the Lu–Hf data only. Error envelopes show 2 SD uncertainties

processes. Furthermore, coefficients of matrix diffusion (Skora et al. 2006; Kohn 2009) and of garnet/matrix partitioning (e.g., Otamendi et al. 2002; Lapen et al. 2003; Kohn 2009) differ significantly for different elements, even among the REE. These differences may control or even inhibit the formation of reaction-induced zoning. Additionally, such zoning may be effectively removed by intracrystalline diffusion (Van Orman et al. 2002; Tirone et al. 2005).

In spite of these complexities, it can be concluded that if Y concentration anomalies (i.e., abrupt variations) occur systematically further from the core than those of V, then either REE uptake by garnet was kinetically or chemically obstructed, or the anomalies do not record a single reaction mechanism. The latter explanation also applies to garnet showing Y-concentration anomalies that are closer to the core than those of V. Trace element profiles of the studied garnet grains, however, show a wide range of negatively correlated V and Y (i.e., and M- to HREE) concentrations. First, this indicates that diffusive rehomogenization of these elements in garnet was not significant. Second, the observation that the concentration of Y, a REE proxy that is expected to diffuse more slowly through the matrix than V, mirrors that of V along garnet growth profiles shows that the uptake of these elements by the growing garnet was apparently not limited by diffusion through the rock matrix (cf. Skora et al. 2006). This, the differences in the position of peak abundance for the different REE relative to the core most likely reflect differences in their garnet/whole-

rock partition coefficients. Furthermore, in the absence of diffusion-limited element uptake, garnet profiles should accurately reflect the changes in matrix composition that occurred as garnet grew. Compositional features common to all samples, such as the synchronized core-to-rim changes in V and Y concentration, suggest that similar metamorphic processes are recorded in the garnet of all samples regardless of grain size. Similarly, changes in concentration trends between garnet generations, e.g., between grt-1a and -1b, may record a specific shift in the reaction mechanism(s) that occurred during garnet growth.

The maximum V content at relatively low concentrations of Y and M- to HREE in grt-1a zones of MS09002a (Fig. 2b) occurs approximately at the transition between taramitic amphibole- and omphacite-bearing inclusion assemblages (core and rim, respectively). As such, the absence of taramitic-amphibole-bearing inclusions and the prograde compositional signature (i.e., high V and V/Y) in garnet from sample MS03005 suggests that it formed exclusively at HP conditions. It is possible that the variations in the concentrations of V, Y, and other elements in prograde garnet were controlled by the presence—and prograde breakdown—of amphiboles belonging to a pre-eclogite assemblage. However, the pre-eclogite assemblage is likely to have contained other phases that may have played an even more important role in the redistribution of the studied trace elements during prograde metamorphism (e.g., titanite, epidote), so interpretations of the observed compositional variations in terms of specific metamorphic processes remain speculative.

Compositional variation across the boundary between grt-1 and grt-2 are relatively abrupt in X-ray maps of Ca (Fig. 2, Supplementary Fig. 2a) and were most likely to have been equally abrupt for the more rapidly diffusing divalent elements (Fe, Mg, and Mn; e.g., Vielzeuf et al. 2007; Perchuk et al. 2009) before their remobilization during thermal overprinting (see maps in Supplementary Fig. 3). Abundances of REE and trace elements such as V and Y in grt-1b zones trend towards the composition of grt-2, indicating that the assemblage controlling the partitioning of elements into the growing garnet did not change significantly between formation of grt-1 and grt-2. This strongly suggests that grt-2 also crystallized at HP conditions.

The age of HP metamorphism

Garnet and omphacite in the studied samples formed during the eclogite stage at estimated peak temperatures of ca. 585–655°C and were subjected to thermal metamorphism after exhumation to upper-crustal levels (Smit et al. 2008). Some temperature estimates for the latter overprint potentially exceed the closure temperature for the Lu–Hf

system (T_c^{Lu-Hf}) in garnet grains of ca. 1 mm in diameter ($\geq 680^\circ\text{C}$; Scherer et al. 2000, using the updated ^{176}Lu decay constant; $\geq 630^\circ\text{C}$; Skora et al. 2008). Despite considerable variation in grain size between and within samples, different grain size fractions comprising both whole garnet grains and garnet fragments lie on Lu–Hf isochrons that yield precise and overlapping ages and show MSWD values close to unity (0.21–1.7). This suggests that (1) all garnet and omphacite grains crystallized—or cooled rapidly—below their T_c^{Lu-Hf} and (2) diffusion during thermal metamorphism and subsequent cooling did not significantly affect their Lu–Hf systematics. The latter indicates either that T_c^{Lu-Hf} is higher than previously estimated or that metamorphic temperatures upon uplift, as calculated by Smit et al. (2008), are overestimated.

As mentioned before, bulk garnet Lu–Hf and Sm–Nd ages represent average ages of all growth zones weighted by their respective Lu and Sm contents. Discrepancies between these ages, resulting from differences in Lu and Sm distribution, can be used to constrain growth histories of monogenetic garnet (e.g., Lapen et al. 2003). In the case of polygenetic garnet, weighted average ages may have little or no geological significance. However, if there is a systematic and resolvable age difference between non-co-genetic garnet zones and the chronometers have remained undisturbed, garnet samples with equivalent growth histories but having variable parent-isotope contributions from different zones (either due to volume or concentration differences) would provide age results that lie on mixing lines between the age components present. Christensen et al. (1989, 1994) have successfully used such an ‘age mixing’ concept to estimate garnet growth rates from centimeter-sized monogenetic garnet crystals, which were physically separated into their constituent growth zones to be individually dated by the Rb–Sr technique. As our samples contained garnet grains that were too small to allow dividing them into separate zones, we have applied a model-based approach. We observed a strong relationship between the Lu–Hf isochron age and X_{Lu}^{grt-2} (Fig. 6), which we interpret to represent a mixing line between the end-member age components of grt-1 and grt-2, whereby age variations primarily reflect the degree of mixing between grt-1 and grt-2 age components, and the age component of grt-2 is identical for each sample. The latter implies that grt-2 zones formed synchronously in all grt-2-bearing samples, presumably by the same process.

The mixing line yields an apparent age of 471.0 ± 0.9 Ma for pure grt-1. This is assumed to be an accurate age estimate for the growth of grt-1 in these samples during metamorphism and eclogitization (M_2^A , following nomenclature of Smit et al. 2008) and provides a better age estimate for this stage than the weighted mean of the overlapping isochron ages (469.9 ± 1.2 Ma), which includes inaccuracy

due to age mixing. There is no resolvable age difference between grt-1a and -1b (Fig. 6b), which implies that all grt-1 crystallized continuously over a time span that is within our estimated precision. This would suggest garnet growth rates that are comparable to those suggested by Christensen et al. (radial growth rates of ca. 0.5–2 mm/Myr; 1989, 1994). Considering that the distribution of Lu relative to garnet nuclei in grt-1 zones varies quite strongly between samples ($X_{\text{Lu}}^{\text{grt-1b}}$ normalized to $X_{\text{Lu}}^{\text{grt-1}} = 0.3\text{--}1.0$), a growth time span for grt-1 in excess of a few Myr would inevitably have resulted in increased scatter relative to the mixing line in Fig. 6a and in a mixing trend in Fig. 6b. The lower intercept at $X_{\text{Lu}}^{\text{grt-2}} = 1$ indicates a ca. 455 Ma age component for grt-2 (Fig. 6a). This age is significantly younger than the age estimate for grt-1 in grt-2-bearing samples and provides an age estimate for a subsequent stage of HP metamorphism (M_2^B). Considering the relatively small volumetric amount of grt-2 and its relatively homogeneous composition, it is likely that its growth duration was short and potentially even shorter than that of grt-1. We note that the precision on the grt-2 age estimate would benefit from precise analyses of garnet having $X_{\text{Lu}}^{\text{grt-2}} > 0.5$. Appropriate samples, however, i.e., eclogites containing garnet dominated by grt-2 zones, were not recognized.

The Lu–Hf age of grt-1 in sample MS03005 (457.9 ± 2.4 Ma), which nucleated and grew exclusively at eclogite facies conditions, is identical to the grt-2 age estimate, supporting the notion that the latter formed at HP conditions. The relatively young age of MS03005 garnet may be related to the deformation history of the sample, considering its extremely well developed S_1 structure. Either the sample represents an older (ca. 470 Ma) eclogite that was dynamically recrystallized at ca. 458 Ma, or eclogitization was delayed for some 15 Myr after burial to HP conditions. We reject the first hypothesis, considering that grt-1 in the sample exhibits concentric growth zoning and lacks typical internal structures that indicate deformation (e.g., healed fractures, sub-grains) and assume that MS03005 remained unequilibrated at HP conditions until it was dynamically eclogitized in response to extreme strain partitioning during M_2^B . This is corroborated by the absence of a prograde growth record in its garnet.

Overall, the data imply that eclogite facies overprinting of the studied rocks occurred during protracted HP metamorphism or during at least two punctuated HP events in the Middle- and Late Ordovician and involved two brief garnet-forming episodes (M_2^A and M_2^B). Multiple HP events seem less plausible because there is no petrological evidence for an intermediate stage of decompression. Most likely, the rocks underwent protracted HP metamorphism during which they underwent differential eclogitization and episodic garnet re-equilibration in response to changes in the P – T – D regime and the influx of fluids.

The relatively low precision of $^{143}\text{Nd}/^{144}\text{Nd}$ and Sm–Nd isochron ages mainly reflects analytical difficulties stemming from the low abundance of Nd in the analyzed separates. Nonetheless, the Sm–Nd ages are often younger than Lu–Hf ages and show negative deviations from the mixing line in Fig. 6. The amphibolite facies overprint, which resulted in the partial rehomogenization of Fe-, Mg-, and Mn throughout the studied garnet grains (Supplementary Fig. 3), is considered to be the main factor that caused resetting of the Sm–Nd system. The large scatter of the Sm–Nd data suggests that the isotope system was only partially reset and that the degree of resetting varies among samples. Sample MS03005, which yielded the youngest Sm–Nd age (430 ± 13 Ma) also shows the largest discrepancy between Lu–Hf and Sm–Nd ages. We speculate that the equigranular fine-grained texture of this specific sample, which resulted from dynamic HP metamorphism, would have provided relatively short diffusion radii, thus allowing more effective resetting of Sm–Nd systematics than in other samples. Therefore, the ca. 430 Ma age should provide the best age estimate for the resetting of the Sm–Nd system in the studied samples. This would imply that the post-eclogite thermal overprint occurred at least 40 Myr after the onset of eclogitization and was approximately synchronous with Scandian (U)HP metamorphism in other parts of the orogen.

The Jæren eclogites and Caledonian geodynamics

In contrast to the well-constrained ages of HP metamorphism for the studied rocks, the crystallization ages of their protoliths remain obscure. No Lu–Hf or Sm–Nd whole-rock isochron could be constructed and the calculation of t_{DM} for both $^{176}\text{Hf}/^{177}\text{Hf}$ and $^{143}\text{Nd}/^{144}\text{Nd}$ did not yield consistent results. The only geochronological constraints available in this context are the U–Pb zircon ages reported for felsic lenses within the eclogites from the Garborg area (ca. 920 and 1,600 Ma; F. Corfu, pers. comm.). These ages are similar to igneous crystallization ages determined for SW Norwegian basement rocks (Schärer et al. 1996; Möller et al. 2002), for basement-related fragments in the Jotun nappe (Schärer 1980) and the Hardangervidda-Ryfylke complex (an allochthonous unit correlating to the studied rocks towards the northwest; Andresen and Færseth 1982), and for allochthonous rocks that occur in the Bergen arcs (e.g., Bingen et al. 2001) and in the WGC (Corfu and Andersen 2002; Walsh et al. 2007). The presence of Proterozoic components in the eclogites indicates either that these rocks are ‘Caledonized’ material derived from the cratonic basement, or suggests that a partial melt derived from Proterozoic source rocks was injected into the protoliths. The geological interpretation of the felsic lenses remains unresolved.

The HP ages presented in this study do not overlap with age estimates for HP metamorphism of the eclogite-bearing terranes in the Bergen area (e.g., 429.9 ± 3.5 Ma, Glodny et al. 2008b) and in Norrbotten (503.5 ± 9.2 Ma; Mørk et al. 1988), and a temporal relationship with the UHP metamorphic cycle of the WGC can also be ruled out (Supplementary Fig. 5). The ca. 455 Ma age of the M_2^B -stage overlaps with the age of eclogites from the Tromsø area (452.1 ± 1.7 Ma; Corfu et al. 2003; Supplementary Fig. 5), but, in contrast to any other eclogite-bearing unit in the orogen, this terrane was metamorphosed in regions proximal to the Laurentic margin (e.g., Brueckner and van Roermund 2004, 2007). The data presented in this study provide the first Middle Ordovician HP age population for the Scandinavian Caledonides. It is not clear whether this age really dates a subduction episode that is unrelated to previously established pre-Scandian eclogite-forming events.

The HP age component of the M_2^B -stage in the studied samples overlaps with the age estimate for HP metamorphism of the JVT in central Sweden (ca. 458 Ma; Brueckner and van Roermund 2007; Supplementary Fig. 5). These authors concluded that their Sm–Nd ages could represent cooling from a thermal maximum that occurred during a preceding metamorphic stage. A correlation with the ca. 500 Ma Finnmarkian orogeny could be excluded because (1) the age data on the JVT seems too consistent to be recording cooling so long after HP metamorphism and (2) the terrane that was most strongly metamorphosed during this stage, the Norrbotten HP terrane, had already been exhumed to upper crustal levels before the end of the Middle Ordovician (Dallmeyer and Gee 1986; Dallmeyer and Stephens 1991; Essex et al. 1997). The ages determined by Brueckner and van Roermund (2007) may record cooling of the JVT after a peak metamorphic stage synchronous with M_2^A . In such a case, the difference between the older Jæren age group (471.0 ± 0.9 Ma) and the HP metamorphism of the JVT (ca. 458 Ma; Supplementary Fig. 5) would either reflect the difference in closure temperature between the Sm–Nd system (used by Brueckner and van Roermund 2007) and the Lu–Hf system applied in this study ($\Delta T_c = 90$ – 230°C ; recalculated using data of Scherer et al. 2000), or show that the JVT underwent a Late Ordovician overprint that disturbed Sm–Nd systematics as observed in the samples dated in this study. Alternatively, the age data might document regional geological variations along the plate-destructive Baltoscandian margin, indicating either (1) that the studied rocks were buried in the same system as the JVT but at an earlier stage or (2) that they underwent a local HP event that arose independently of JVT subduction. The latter option is highly plausible when considering palaeogeography. Throughout the Ordovician, the southwestern margin of Baltica was separated from the

protocontinent Avalonia by a contracting oceanic domain, the Tornquist Sea. Across the British Isles, northeastern Europe, and southern Scandinavia, Ordovician facies shifts in sedimentary successions and arc-related volcanic rocks in the Avalonian foreland record the closure of this ocean, which resulted in the subduction of the Baltoscandian margin underneath Avalonia and the docking of the latter to the BCS during the Late Ordovician (Pharaoh et al. 1993; Cocks et al. 1997; Torsvik and Rehnström 2003). This tectonic event is recorded along the Scandinavian Tornquist zone, i.e., in rocks that constitute—or are derived from—the southwestern segment of the BCS (e.g., Torsvik and Rehnström 2003). Considering the geographical position and the metamorphic age of the studied rocks, it is highly likely that these were reworked in a subduction system that accommodated Avalonia–Baltica convergence. If this system was—or became—tectonically related to the JVT subduction zone, the studied rocks would document a local imprint of the Ordovician subduction stage that was identified as the ‘Jämtlandian’ by Brueckner and van Roermund (2007). It would imply that this stage has a more extensive lateral imprint (>600 km) and affected rocks over a wider tectono-stratigraphic range than previously thought. This suggestion, originally made by Brueckner and van Roermund (2004), is supported by Late Ordovician cooling ages from the allochthonous Høyvik group in western Norway (Andersen et al. 1998; Eide et al. 1999) and by the Ordovician U–Pb zircon and monazite ages from eclogite-bearing allochthons that juxtapose the WGC (Walsh et al. 2007). The Sm–Nd data from the studied rocks suggest that exhumation to upper crustal levels was accomplished at the onset of the Scandian episode (ca. 430 Ma). This would be in concurrence with the timing of exhumation and lateral transport of the JVT, the Høyvik group, and several other allochthonous terranes in the central and southern Caledonides (e.g., Tucker et al. 2004; Hacker and Gans 2005). The post-eclogite history of the studied rocks will be elaborated on in a follow-up study.

Conclusions

Application of Lu–Hf and Sm–Nd geochronology to eclogites from the Jæren nappe, SW Scandinavian Caledonides, indicates that these rocks were affected by protracted HP metamorphism involving two brief episodes of garnet growth during the Middle and Late Ordovician. Five out of the six studied eclogite samples provided Lu–Hf ages of ca. 470 Ma. One sample yielded a younger age of 457.9 ± 2.4 Ma (± 2 SD). Major- and trace element analyses showed that garnet in the younger sample comprises a single growth zone. Garnet porphyroblasts from the other samples have two growth zones that have distinct chemical

compositions. The cores show a major- and trace element composition that is similar to that of garnet in the younger sample. Taking into account the Lu-contributions of individual zones allows age estimates of 471.0 ± 0.9 Ma for the cores of these grains and ca. 455 Ma age for the rims. The results presented in this study either document a hitherto unknown eclogite facies stage in the Caledonian Wilson Cycle, or provide a new and more-detailed picture of the HP event than has been deduced elsewhere in the orogen by means of other isotope systems. Furthermore, this study illustrates the complexities and advantages of garnet geochronology and shows the strength of Lu–Hf dating for uncovering the geochronological record of eclogites.

Acknowledgments We thank J. Berndt for assistance on the EPMA and the LA-ICP-MS, M. Menneken for help on the Raman spectrometer, E. Janots for constructive criticism, and E. Kooijman for her efforts in the field. Thanks are also due to P. Löbke for sample preparation and H. Baier for her kind help in the laboratory. We acknowledge C. Majjer for providing us with crucial information on the field locality and F. Corfu for generously sharing his preliminary U–Pb results. The constructive reviews of T. J. Lapen and B.R. Hacker and editorial handling by J. Hoefs were highly appreciated. Financial support by the Deutsche Forschungsgemeinschaft (DFG) is gratefully acknowledged (grant BR 1068/14-1).

References

- Andersen TB, Berry HN, Lux DR, Andresen A (1998) The tectonic significance of pre-Scandian $^{40}\text{Ar}/^{39}\text{Ar}$ phengite cooling ages in the Caledonides of western Norway. *J Geol Soc Lond* 155:297–309
- Andréasson PG, Gee DG, Sukotji S (1985) Seve eclogites in the Norrbotten Caledonides, Sweden. In: Gee DG, Sturt BA (eds) *The Caledonide Orogen: Scandinavia and related areas*. Wiley, Chichester, pp 887–901
- Andresen A, Færseth R (1982) An evolutionary model for the southwest Norwegian Caledonides. *Am J Sci* 282:756–782
- Austrheim H (1987) Eclogitization of lower crustal granulites by fluid migration through shear zones. *Earth Planet Sci Lett* 81:221–232
- Begemann F, Ludwig KR, Lugmair GW, Min K, Nyquist LE, Patchett PJ, Renne PR, Shih C-Y, Villa IM, Walker J (2001) Call for an improved set of decay constants for geochronological use. *Geochim Cosmochim Acta* 65:111–121
- Bingen B, van Breemen O (1998) U–Pb monazite ages in amphibolite- to granulite-facies orthogneiss reflect hydrous mineral breakdown reactions: Sveconorwegian Province of SW Norway. *Contrib Mineral Petrol* 132:336–353
- Bingen B, Demaiffe D, van Breemen O (1998) The 616 Ma old Egersund basaltic dike swarm, SW Norway, and Late Neoproterozoic opening of the Iapetus Ocean. *J Geol* 106:565–574
- Bingen B, Davis WJ, Austrheim H (2001) Zircon U–Pb geochronology in the Bergen arc eclogites and their Proterozoic protoliths, and implications for the pre-Scandian evolution of the Caledonides in western Norway. *Geol Soc Am Bull* 113:640–649
- Bingen B, Austrheim H, Whitehouse MJ, Davis WJ (2004) Trace element signature and U–Pb geochronology of eclogite-facies zircon, Bergen Arcs, Caledonides of W Norway. *Contrib Mineral Petrol* 147:671–683
- Birkeland T (1981) The geology of Jæren and adjacent districts. A contribution to the Caledonian nappe tectonics of Rogaland, southwest Norway. *Norsk Geol Tidsskr* 61:213–235
- Bizzarro M, Baker JA, Haack H, Ulfbeck D, Rosing M (2003) Early history of Earth’s crust-mantle system inferred from hafnium isotopes in chondrites. *Nature* 421:931–933
- Bouvier A, Vervoort JD, Patchett PJ (2008) The Lu–Hf and Sm–Nd isotopic composition of CHUR: Constraints from unequilibrated chondrites and implications for the bulk composition of terrestrial planets. *Earth Planet Sci Lett* 273:48–57
- Boynton WV (1984) Cosmochemistry of the rare earth elements: meteorite studies. In: Henderson P (ed) *Rare earth element geochemistry*. Elsevier, Amsterdam, pp 63–114
- Brueckner HK, van Roermund HLM (2004) Dunk tectonics: a multiple subduction/duction model for the evolution of the Scandinavian Caledonides. *Tectonics* 23:TC2004:1–20
- Brueckner HK, van Roermund HLM (2007) Concurrent HP metamorphism on both margins of Iapetus: Ordovician ages for eclogites and garnet pyroxenites from the Seve Nappe Complex, Swedish Caledonides. *J Geol Soc London* 164:117–128
- Bryhni I, Andréasson P-G (1985) Metamorphism in the Scandinavian Caledonides. In: Gee DG, Sturt BA (eds) *The Caledonide Orogen: Scandinavia and related areas*. Wiley, Chichester, pp 763–781
- Carswell DA, Brueckner HK, Cuthbert SJ, Mehta K, O’Brien PJ (2003) The timing of stabilization and the exhumation rate for ultra-high pressure rocks in the Western Gneiss Region of Norway. *J Metamorph Geol* 21:601–612
- Christensen JN, Rosenfeld JL, DePaolo DJ (1989) Rates of tectonometamorphic processes from rubidium and strontium isotopes in garnet. *Science* 244:1465–1469
- Christensen JN, Selverstone J, Rosenfeld JL, DePaolo DJ (1994) Correlation by Rb–Sr geochronology of garnet growth histories from different structural levels within the Tauern Window, Eastern Alps. *Contrib Mineral Petrol* 118:1–12
- Cocks LRM, McKerrow WS, van Staal CR (1997) The margins of Avalonia. *Geol Mag* 134:627–636
- Corfu F, Andersen TB (2002) U–Pb ages of the Dalsfjord Complex, SW Norway, and their bearing on the correlation of allochthonous crystalline segments of the Scandinavian Caledonides. *Int J Earth Sci* 91:955–963
- Corfu F, Ravna EJK, Kullerud K (2003) A late Ordovician U–Pb age for the Tromsø Nappe eclogites, uppermost Allochthon of the Scandinavian Caledonides. *Contrib Mineral Petrol* 145:502–513
- Cuthbert SJ, Carswell DA, Krogh-Ravna EJ, Wain A (2000) Eclogites and eclogites in the Western Gneiss Region, Norwegian Caledonides. *Lithos* 52:165–195
- Dallmeyer RD, Gee DG (1986) $^{40}\text{Ar}/^{39}\text{Ar}$ mineral age record of early Caledonian tectonothermal activity in the Baltoscandian miogeocline: implications for a polyphase Caledonian orogenic evolution. *Geol Soc Am Bull* 97:26–34
- Dallmeyer RD, Stephens MB (1991) Chronology of eclogite retrogression within the Seve Nappe Complex, Råvvejaure, Sweden: evidence from $^{40}\text{Ar}/^{39}\text{Ar}$ mineral ages. *Geol Rundsch* 80:729–743
- Dunning GR, Pedersen RB (1988) U/Pb ages of ophiolites and arc-related plutons of the Norwegian Caledonides: implications for the development of Iapetus. *Contrib Mineral Petrol* 98:13–23
- Eide EA, Torsvik TH, Andersen TB, Arnaud NO (1999) Early carboniferous unroofing in western Norway: a tale of alkali feldspar thermochronology. *J Geol* 107:353–374
- Essex RM, Gromet LP, Andréasson P-G, Albrecht LG (1997) Early Ordovician U–Pb metamorphic ages of the eclogite-bearing Seve nappes, Northern Scandinavian Caledonides. *J Metamorph Geol* 15:665–676
- Falkum T (1982) Geologisk kart over Norge, Berggrunnskart Mandal 1:250.000. Norges Geol Unders, Trondheim

- Glodny J, Kühn A, Austrheim H (2002) Rb/Sr record of fluid-rock interaction in eclogites, Bergen Arcs, Norway. *Geochim Cosmochim Acta* 66(S1):A280
- Glodny J, Kühn A, Austrheim H (2008a) Diffusion versus recrystallization processes in Rb–Sr geochronology: isotopic relics in eclogite facies rocks, Western Gneiss Region, Norway. *Geochim Cosmochim Acta* 72:506–525
- Glodny J, Kühn A, Austrheim H (2008b) Geochronology of fluid-induced eclogite and amphibolite facies metamorphic reactions in a subduction-collision system, Bergen Arcs, Norway. *Contrib Mineral Petrol* 156:27–48
- Griffin WL, Brueckner HK (1980) Caledonian Sm–Nd ages and a crustal origin for Norwegian eclogites. *Nature* 285:319–321
- Griffin WL, Austrheim H, Brastad K, Bryhni I, Krill AG, Krogh EJ, Mørk MBE, Qvale H, Tørudbakken B (1985) High-pressure metamorphism in the Scandinavian Caledonides. In: Gee DG, Sturt BA (eds) *The Caledonide Orogen: Scandinavia and related areas*. Wiley, Chichester, pp 783–801
- Hacker BR, Gans PB (2005) Continental collisions and the creation of ultrahigh-pressure terranes: petrology thermochronology of nappes in the central Scandinavian Caledonides. *Geol Soc Am Bull* 117:117–134
- Hermann J (2002) Allanite: thorium and light rare earth element carrier in subducted crust. *Chem Geol* 192:289–306
- Hickmott DD, Shimizu N, Spear FS, Selverstone J (1987) Trace-element zoning in a metamorphic garnet. *Geology* 15:573–576
- Jamtveit B, Bucher-Nurminen K, Austrheim H (1990) Fluid controlled eclogitization of granulites in deep crustal shear zones, Bergen arcs, Western Norway. *Contrib Mineral Petrol* 104:184–193
- Jochum KP, Willbold M, Raczek I, Stoll B, Herwig K (2005) Chemical characterisation of the USGS reference glasses GSA-1G, GSC-1G, GSD-1G, GSE-1G, BCR-2G, BHVO-2G and BIR-1G using EPMA, ID-TIMS, ID-ICP-MS and LA-ICP-MS. *Geostand Geoanalyst Res* 29:285–302
- Kohn MJ (2009) Models of garnet differential geochronology. *Geochim Cosmochim Acta* 73:170–182
- Konrad-Schmolke M, Zack T, O'Brien PJ, Jakob DE (2009) Combined thermodynamic and rare earth element modelling of garnet growth during subduction: examples from ultrahigh-pressure eclogite of the Western Gneiss Region, Norway. *Earth Planet Sci Lett* 272:488–498
- Krogh EJ (1977) Evidence of Precambrian continent–continent collision in Western Norway. *Nature* 267:17–19
- Krogh EJ, Andresen A, Bryhni I, Broks TM, Kristensen SE (1990) Eclogites and polyphase *P–T* cycling in the Caledonian uppermost allochthon in Troms, northern Norway. *J Metamorph Geol* 8:289–309
- Krogh-Ravna EJ, Roux MRM (2006) Metamorphic evolution of the Tønsvika eclogite, Tromsø nappe—evidence for a new UHPM province in the Scandinavian Caledonides. *Int Geol Rev* 48:861–881
- Kühn A, Glodny J, Austrheim H, Råheim A (2002) The Caledonian tectono-metamorphic evolution of the Lindås Nappe: constraints from U–Pb, Sm–Nd and Rb–Sr ages of granitoid dykes. *Norsk Geol Tidsskr* 82:45–57
- Kylander-Clark ARC, Hacker BR, Johnson CM, Beard BL, Mahlen NJ, Lapen TJ (2007) Coupled Lu–Hf and Sm–Nd geochronology constrains prograde and exhumation histories of high- and ultrahigh-pressure eclogites from western Norway. *Chem Geol* 242:137–154
- Kylander-Clark ARC, Hacker BR, Mattinson JM (2008) Slow exhumation of UHP terranes: titanite and rutile ages of the Western Gneiss Region, Norway. *Earth Planet Sci Lett* 272:531–540
- Kylander-Clark ARC, Hacker BR, Johnson CM, Beard BL, Mahlen NJ (2009) Slow subduction of a thick ultrahigh-pressure terrane. *Tectonics* 28:TC2003:1–14
- Lapen TJ, Johnson CM, Baumgartner LP, Mahlen NJ, Beard BL, Amato JM (2003) Burial rates during prograde metamorphism of an ultra-high-pressure terrane: an example from Lago di Cignana, western Alps, Italy. *Earth Planet Sci Lett* 215:57–72
- Ludwig KR (2005) User's Manual for ISOPLOT/3.27. A geochronological toolkit for Microsoft Excel. Berkeley Geochronology Center Spec Pub, p 71
- Maijer C, Hermans GAEM, Tobi AC, Jansen JBH (1987) Day 10—Caledonides and westernmost Precambrian intrusions. In: Maijer C, Padget P (eds) *The geology of southernmost Norway: an excursion guide*. *Nor Geol Unders Spec Publ* 1:99–104
- Maijer C, Jansen JBH, Verschure RH, Senior A (1990) Excursion log of the southernmost Caledonian meta-eclogites and the westernmost Precambrian intrusives in Norway. In: *Excursion Guide to the 19th Nordic Geological Winter Meeting*, Stavanger, January 1990, pp 1–12
- Möller A, O'Brien PJ, Kennedy A, Kröner A (2002) Polyphase zircon in ultrahigh-temperature granulites (Rogaland, SW Norway): constraints for Pb diffusion in zircon. *J Metamorph Geol* 20:727–740
- Mørk MBE, Kullerød K, Stabel A (1988) Sm–Nd dating of Seve eclogites, Norrbotten, Sweden—Evidence for early Caledonian (505 Ma) subduction. *Contrib Mineral Petrol* 99:344–351
- Münker C, Weyer S, Scherer EE, Mezger K (2001) Separation of high field strength elements (Nb, Ta, Zr, Hf) and Lu from rock samples for MS-ICPMS measurements. *Geochem Geophys Geosyst* 2. doi:10.1029/2001GC000183
- Otamendi JE, de la Rosa JD, Patiño Douce AE, Castro A (2002) Rayleigh fractionation of heavy rare earths and yttrium during metamorphic garnet growth. *Geology* 30:159–162
- Pearce NJG, Perkins WT, Westgate JA, Gorton MP, Jackson SE, Neal CR, Chenery SP (1997) A compilation of new and published major and trace element data for NIST SRM 610 and NIST SRM 612 glass reference materials. *Geostand Geoanalyst Res* 21:115–144
- Perchuk AL, Burchard M, Schertl H-P, Maresch WV, Gerya TV, Bernhardt H-J, Vidal O (2009) Diffusion of divalent cations in garnet: multi-couple experiments. *Contrib Mineral Petrol* 157:573–592
- Pharaoh TC, Brewer TS, Webb PC (1993) Subduction-related magmatism of Late Ordovician age in eastern England. *Geol Mag* 130:647–656
- Roberts D, Gee DG (1985) An introduction to the structure of the Scandinavian Caledonides. In: Gee DG, Sturt BA (eds) *The Caledonide Orogen: Scandinavia and related areas*. Wiley, Chichester, pp 55–68
- Roddick JC, Jorde K (1981) Rb–Sr whole rock isochron dates on rocks of the Jæren district, SW Norway. *Nor Geol Unders* 365:55–67
- Root DB, Hacker BR, Mattinson JM, Wooden JL (2004) Zircon geochronology and ca. 400 Ma exhumation of Norwegian ultrahigh-pressure rocks: an ion microprobe and chemical abrasion study. *Earth Planet Sci Lett* 228:325–341
- Root DB, Hacker BR, Gans PB, Ducea MN, Eide EA, Mosenfelder JL (2005) Discrete ultrahigh-pressure domains in the Western Gneiss Region, Norway: implications for formation and exhumation. *J Metamorph Geol* 23:45–61
- Scambelluri M, Pettke T, van Roermund HLM (2009) Majoritic garnet monitor deep subduction fluid flow and mantle dynamics. *Geology* 36:59–62
- Schärer U (1980) U–Pb and Rb–Sr dating of a polymetamorphic nappe terrain: The Caledonian Jotun Nappe, southwestern Norway. *Earth Planet Sci Lett* 49:205–218
- Schärer U, Wilmart E, Duchesne JC (1996) The short duration and anorogenic character of anorthosite magmatism: U–Pb dating of the Rogaland complex, Norway. *Earth Planet Sci Lett* 139:335–350

- Scherer EE, Cameron KL, Blichert-Toft J (2000) Lu–Hf garnet geochronology: closure temperature relative to the Sm–Nd system and the effects of trace mineral inclusions. *Geochim Cosmochim Acta* 64:3413–3432
- Scherer EE, Münker C, Mezger K (2001) Calibration of the lutetium–hafnium clock. *Science* 295:683–686
- Scherer EE, Mezger K, Münker C (2003) The ^{176}Lu decay constant discrepancy: terrestrial samples vs. meteorites. *Meteorit Planet Sci* 38(Suppl A136)
- Shannon RD (1976) Revised effective ionic radii and systematic studies of interatomic distances in halides and chalcogenides. *Acta Crystallogr A* 32:751–767
- Skora S, Baumgartner LP, Mahlen NJ, Johnson CM, Pilet S, Hellebrand E (2006) Diffusion-limited REE uptake by eclogite garnets and its consequences for Lu–Hf and Sm–Nd geochronology. *Contrib Mineral Petrol* 152:703–720
- Skora S, Baumgartner LP, Mahlen NJ, Lapen TJ, Johnson CM, Bussy F (2008) Estimation of a maximum Lu diffusion rate in a natural eclogite garnet. *Swiss J Geosci*. doi:10.1007/s00015-008-1268-y
- Smit MA, Bröcker M, Scherer EE (2008) Aragonite and magnesite in eclogites from the Jæren nappe, SW Norway: Disequilibrium in the system $\text{CaCO}_3\text{--MgCO}_3$ and its petrological implications. *J Metamorph Geol* 26:959–979
- Söderlund U, Patchett PJ, Vervoort JD, Isachsen CE (2004) The ^{176}Lu decay constant determined by Lu–Hf and U–Pb isotope systematics of Precambrian mafic intrusions. *Earth Planet Sci Lett* 219:311–324
- Spengler D, Brueckner HK, van Roermund HLM, Drury MR, Mason PRD (2009) Long-lived, cold burial of Baltica to 200 km depth. *Earth Planet Sci Lett* 281:27–35
- Sturt BA, Thon A (1978) An ophiolite complex of probable early Caledonian age discovered on Karmøy. *Nature* 275:538–539
- Terry MP, Robinson P (2004) Geometry of eclogite-facies structural features: implications for production and exhumation of ultra-high-pressure and high-pressure rocks, Western Gneiss Region, Norway. *Tectonics* 23:TC2001:1–23
- Tirone M, Ganguly J, Dohmen R, Langenhorst F, Hervig R, Becker H-W (2005) Rare earth diffusion kinetics in garnet: experimental studies and applications. *Geochim Cosmochim Acta* 69:2385–2398
- Torsvik TH, Rehnström EF (2003) The Tornquist Sea and Baltica–Avalonia docking. *Tectonophysics* 362:67–82
- Tucker RD, Krogh TE, Råheim A (1990) Proterozoic evolution and age-province boundaries in the central part of the Western Gneiss region, Norway: results of U–Pb dating of accessory minerals from Trondheimsfjord to Geiranger. In: Gower CF, Rivers T, Ryan B (eds) *Mid-Proterozoic Laurentia–Baltica*. *Geol Assoc Can Spec Paper* 38:149–173
- Tucker RD, Robinson P, Solli A, Gee DG, Thorsnes T, Krogh TE, Nordgulen Ø, Bickford ME (2004) Thrusting and extension in the Scandian hinterland, Norway: New U–Pb ages and tectono-stratigraphic evidence. *Am J Sci* 304:477–532
- Van Orman JA, Grove TL, Shimizu N, Layne GD (2002) Rare earth diffusion in a natural pyrope single crystal at 2.8 GPa. *Contrib Mineral Petrol* 142:416–424
- Van Roermund HLM (1985) Eclogites of the Seve Nappe, central Scandinavian Caledonides. In: Gee DG, Sturt BA (eds) *The Caledonide Orogen: Scandinavia and related areas*. Wiley, Chichester, pp 873–886
- Van Roermund HLM (2009) Recent progress in Scandian ultrahigh-pressure metamorphism in the northernmost domain of the Western Gneiss Complex, SW Norway: continental subduction down to 180–200 km depth. *J Geol Soc Lon* 166:739–751
- Verschure RH, Andriessen PAM, Boelrijk NAIM, Hebeda EH, Maijer C, Priem HNA, Verdurmen EAT (1980) On the thermal stability of Rb–Sr and K–Ar biotite systems: evidence from coexisting Sveconorwegian (ca 870 Ma) and Caledonian (ca 400 Ma) biotites in SW Norway. *Contrib Mineral Petrol* 74:245–252
- Vielzeuf D, Baronnet A, Perchuk AL, Laporte D, Baker MB (2007) Calcium diffusivity in aluminosilicate garnets: an experimental and ATEM study. *Contrib Mineral Petrol* 154:153–170
- Walsh EO, Hacker BR, Gans PB, Grove M, Gehrels G (2007) Protolith ages and exhumation histories of (ultra)high-pressure rocks across the Western Gneiss Region, Norway. *Geol Soc Am Bull* 119:289–301